AUTHOR QUERY FORM

ELSEVIER	**Journal: STOTEN** **Article Number: 21822**	**Please e-mail your responses and any corrections to:** **E-mail: Corrections.ESCH@elsevier.spitech.com**

Dear Author,

Please check your proof carefully and mark all corrections at the appropriate place in the proof (e.g., by using on-screen annotation in the PDF file) or compile them in a separate list. Note: if you opt to annotate the file with software other than Adobe Reader then please also highlight the appropriate place in the PDF file. To ensure fast publication of your paper please return your corrections within 48 hours.

For correction or revision of any artwork, please consult http://www.elsevier.com/artworkinstructions.

We were unable to process your file(s) fully electronically and have proceeded by

☐ Scanning (parts of) your article ☐ Rekeying (parts of) your article ☐ Scanning the artwork

No queries have arisen during the processing of your article.

Thank you for your assistance.

Supplementary material

Science of the Total Environment xxx (2017) xxx–xxx

Contents lists available at ScienceDirect

Science of the Total Environment

journal homepage: www.elsevier.com/locate/scitotenv

Understanding controls on redox processes in floodplain sediments of the Upper Colorado River Basin

Vincent Noël [a], Kristin Boye [a,b], Ravi K. Kukkadapu [c], Sharon Bone [a], Juan S. Lezama Pacheco [a,b], Emily Cardarelli [b], Noémie Janot [a], Scott Fendorf [b], Kenneth H. Williams [d], John R. Bargar [a,*]

[a] Stanford Synchrotron Radiation Lightsource, SLAC National Accelerator Laboratory, Menlo Park, CA 94025, United States
[b] Department of Environmental Earth System Science, Stanford University, Stanford, CA 94305, United States
[c] Environmental Molecular Sciences Laboratory, Pacific Northwest National Laboratory, Richland, WA 99354, United States
[d] Earth Sciences Division, Lawrence Berkeley National Laboratory, Berkeley, CA 94720, United States

HIGHLIGHTS

- Organic-enriched sediments are common in Upper Colorado River Basin floodplains.
- Reducing conditions are maintained primarily by organic carbon content and moisture
- Particle size governs reactive S(0) and FeS species by mediating oxidant diffusion.
- Organic-enriched sediments mediate groundwater contaminants in floodplains.

GRAPHICAL ABSTRACT

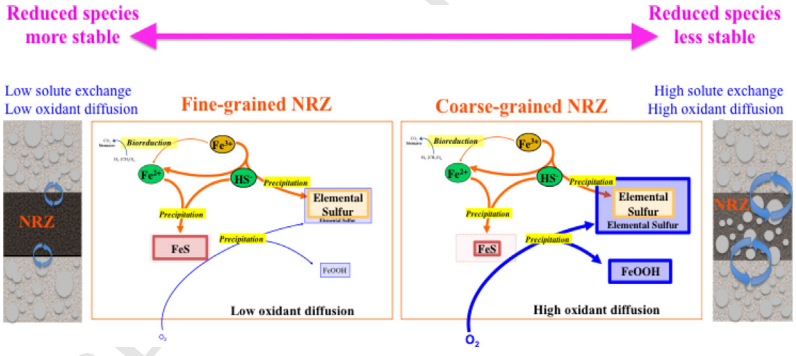

ARTICLE INFO

Article history:
Received 19 October 2016
Received in revised form 16 January 2017
Accepted 16 January 2017
Available online xxxx

Editor: F.M. Tack

Keywords:
Floodplain sediments
Redox processes
Iron and sulfur
X-ray absorption spectroscopy
Upper Colorado River Basin

ABSTRACT

Floodplains, heavily used for water supplies, housing, agriculture, mining, and industry, are important repositories of organic carbon, nutrients, and metal contaminants. The accumulation and release of these species is often mediated by redox processes. Understanding the physicochemical, hydrological, and biogeochemical controls on the distribution and variability of sediment redox conditions is therefore critical to developing conceptual and numerical models of contaminant transport within floodplains. The Upper Colorado River Basin (UCRB) is impacted by former uranium and vanadium ore processing, resulting in contamination by V, Cr, Mn, As, Se, Mo and U. Previous authors have suggested that sediment redox activity occurring within organic carbon-enriched bodies located below the groundwater level may be regionally important to the maintenance and release of contaminant inventories, particularly uranium. To help assess this hypothesis, vertical distributions of Fe and S redox states and sulfide mineralogy were assessed in sediment cores from three floodplain sites spanning a 250 km transect of the central UCRB.

The results of this study support the hypothesis that organic-enriched reduced sediments are important zones of biogeochemical activity within UCRB floodplains. We found that the presence of organic carbon, together with pore saturation, are the key requirements for maintaining reducing conditions, which were dominated by sulfate-reduction products. Sediment texture was found to be of secondary importance and to moderate the

Abbreviations: SSRL, Stanford Synchrotron Radiation Lightsource; XAS, X-ray absorption spectroscopy; XANES, X-ray Absorption Near Edge Structure; EXAFS, X-ray Absorption Fine Structure; LC-LS, linear combination-least squares; RT, room temperature; bgs, below ground surface; OC, organic carbon; UCRB, Upper Colorado River Basin; OEZ, organic-enriched zones; NRZ, naturally reduced zones.

* Corresponding author.
E-mail address: bargar@slac.stanford.edu (J.R. Bargar).

http://dx.doi.org/10.1016/j.scitotenv.2017.01.109
0048-9697/

response of the system to external forcing, such as oxidant diffusion. Consequently, fine-grain sediments are relatively resistant to oxidation in comparison to coarser-grained sediments. Exposure to oxidants consumes precipitated sulfides, with a disproportionate loss of mackinawite (FeS) as compared to the more stable pyrite. The accompanying loss of redox buffering capacity creates the potential for release of sequestered radionuclides and metals. Because of their redox reactivity and stores of metals, C, and N, organic-enriched sediments are likely to be important to nutrient and contaminant mobility within UCRB floodplain aquifers.

1. Introduction

Floodplains are estimated to cover up to 1.5% of the terrestrial surface, and constitute important links between surface and subsurface (Chaopricha and Marín-Spiotta, 2014; Blazejewski et al., 2009). Floodplains act as buffers for flood water and as filters for nutrients and pollutants carried with river water and sediment from upstream source areas. Conversely, river-floodplain sediment systems, heavily used for water supplies, housing, agriculture, mining, and industry, can be long-term sinks for heavy metal contaminants. In this context, sediment-water interactions within floodplains can attenuate or accentuate nutrient and pollutant loads in groundwater (Naiman and Décamps, 1997; Tockner and Stanford, 2002; Pinay et al., 1991; Tabacchi et al., 1998). This behavior is particularly important within the Upper Colorado River Basin (UCRB), where groundwater discharge contributes the majority of total net surface outflow (Miller et al., 2016). In combination with subsurface or hyporheic exchange, groundwater discharge regulates surface water quality (Findlay, 1995). Floodplain sediments exhibit sharp lithologic heterogeneity (Janot et al., 2016). The high heterogeneity of sediment textures and chemical/mineralogical compositions creates chemical gradients that physically juxtapose oxidizing and reducing conditions (Tockner et al., 2010). The stability of contaminants within such sediments is closely linked to redox conditions (Lynch et al., 2014; Schulz-Zunkel et al., 2015). Transport of oxidants and contaminants, including As, Sb, Se, Cr, As, Hg and U, across these heterogeneities drives toxicant accumulation or release (Hua and Deng, 2008; Burton et al., 2011; Hyun et al., 2012; Veeramani et al., 2013). Knowledge of the spatial, hydrological, mineralogical, and biogeochemical controls over redox conditions is therefore critical for understanding the function of floodplain sediments as sinks or supplies of inorganic contaminants. The aim of this work was to contribute to the development of regionally-relevant conceptual models of the biogeochemical function of organic-enriched sediments.

Previous studies suggested that sediment moisture is important for maintenance of reducing conditions in floodplain sediments within the Upper Colorado River Basin (UCRB) (Janot et al., 2016; Campbell et al., 2012). Significantly, within this region, water tables exhibit strong seasonal fluctuation tied to early summer meltwater discharges, which temporarily displace the capillary fringe upwards. The subsequent filling of pore space by water creates the potential for the onset of Fe(III) and sulfate reducing conditions. Thus, seasonal hydrological variations drive cyclic changes of redox conditions (Lair et al., 2009; Weber et al., 2009; Lynch et al., 2014; Schulz-Zunkel et al., 2015). Iron and sulfur mineral transformations (dissolution/precipitation of sulfides and oxides) are driven by these hydrologic changes (Shuman, 1997; Ford et al., 1997; Rickard and Luther, 2007; Qafoku et al., 2009; Canfield et al., 1992; Noël et al., 2014). Consequently, the chemical forms of S and Fe exhibit dramatic variability tied to redox conditions, providing efficient and precise biogeochemical tracers of redox processes.

UCRB floodplain sites are widely impacted by former U ore processing activities. At the Rifle, CO, site, U concentrations >200-fold higher than background concentrations are found within layers of fine-grained, clay-rich sediments having markedly higher organic C content than the sand and cobble alluvium that dominates the floodplain (Janot et al., 2016; Qafoku et al., 2014; Campbell et al., 2012). These sediments may exhibit black coloration from sulfidic mineral precipitation, indicating strongly sulfate reducing conditions, and therefore, have been referred to as 'naturally reduced zones' or NRZs (Campbell et al., 2012). They are suspected to play an important role in maintaining the persistent groundwater U contamination plume at the Rifle site (Janot et al., 2016). Janot et al. noted that other floodplains within the UCRB exhibit similar sediment characteristics, and predicted that sulfidic NRZs are regionally common and responsible for the accumulation of U at other contaminated floodplain sites (Blazejewski et al., 2009; Janot et al., 2016). This hypothesis is supported by similar groundwater compositions in upper CRB aquifers with high sulfate concentrations around 250 mg/L (Report of Department of Energy, 1999, 2003, 2011, 2013). Thus, it was posited that the behavior of the fine-grained, water-saturated NRZs observed at Rifle could be used as a model to understand the functioning of floodplain dynamics and predict contaminant behavior regionally. If correct, this model would provide a valuable tool to understand reduced sediment biogeochemistry and to rationalize and manage the many data-poor U-contaminated floodplain sites within the UCRB.

The objective of this study was to test the validity of the 'Rifle model' of NRZs, starting with a survey across the floodplain at the Rifle site, and extending it to other U-contaminated UCRB floodplain sites managed by the Department of Energy (DOE) Office of Legacy Management. Prior knowledge suggests that reduced sediments are present also at the Grand Junction and Naturita sites (CO) (Davis et al., 2006). The inclusion of these two sites extends the study area to cover a linear distance of 250 km on the Colorado river in the central portion of the UCRB. This study further intended to improve our knowledge of the biogeochemical controls over Fe and S mineralization in order to develop a regionally consistent model of Fe and S redox processes in the UCRB floodplain sediments.

2. Materials and methods

2.1. Field sites, sample collection

The field sites are located on US DOE legacy sites on floodplains in the UCRB (Fig. 1). More information on field sites is available in the Appendix A. Rotosonic drilling (Rifle) or direct push coring (Grand Junction, Naturita) were used to recover intact floodplain sediment cores (in 1.5 m intervals). Recovered cores were cased in N_2-purged plastic tubes. In this study, 4 cores consisted of NRZs were selected from the three field sites; 2 cores (748 and 753) from Rifle, 1 core (GJAST15B) from Grand Junction and 1 core (NAT-M8-1) from Naturita. For each core, the sediment samples were collected every 10 to 40 cm from surface to bedrock (ca. 9.3 m bgs for Rifle, and 5–6 m bgs for Grand Junction and Naturita) (Janot et al., 2016). Pebbles and cobbles larger than about 10 mm were removed, and the remaining sediments were immediately placed into containers. The sediment samples that visibly appeared to be darkened by the presence of sulfides and smelled sulfidic were collected at relatively fine vertical resolution (~5 cm), along with a segment of neighboring over- and underlying sediment, under Ar flow and preserved from oxidation in Ar-purged serum vials (crimp-sealed with rubber stoppers) (Fig. S1). All samples were immediately stored in the dark at 3 °C, and shipped on ice to the laboratory where they were introduced in a glove box in 5%H_2/95%N_2 atmosphere in order to be vacuum-dried. After drying, each sediment sample was

Please cite this article as: Noël, V., et al., Understanding controls on redox processes in floodplain sediments of the Upper Colorado River Basin, Sci Total Environ (2017), http://dx.doi.org/10.1016/j.scitotenv.2017.01.109

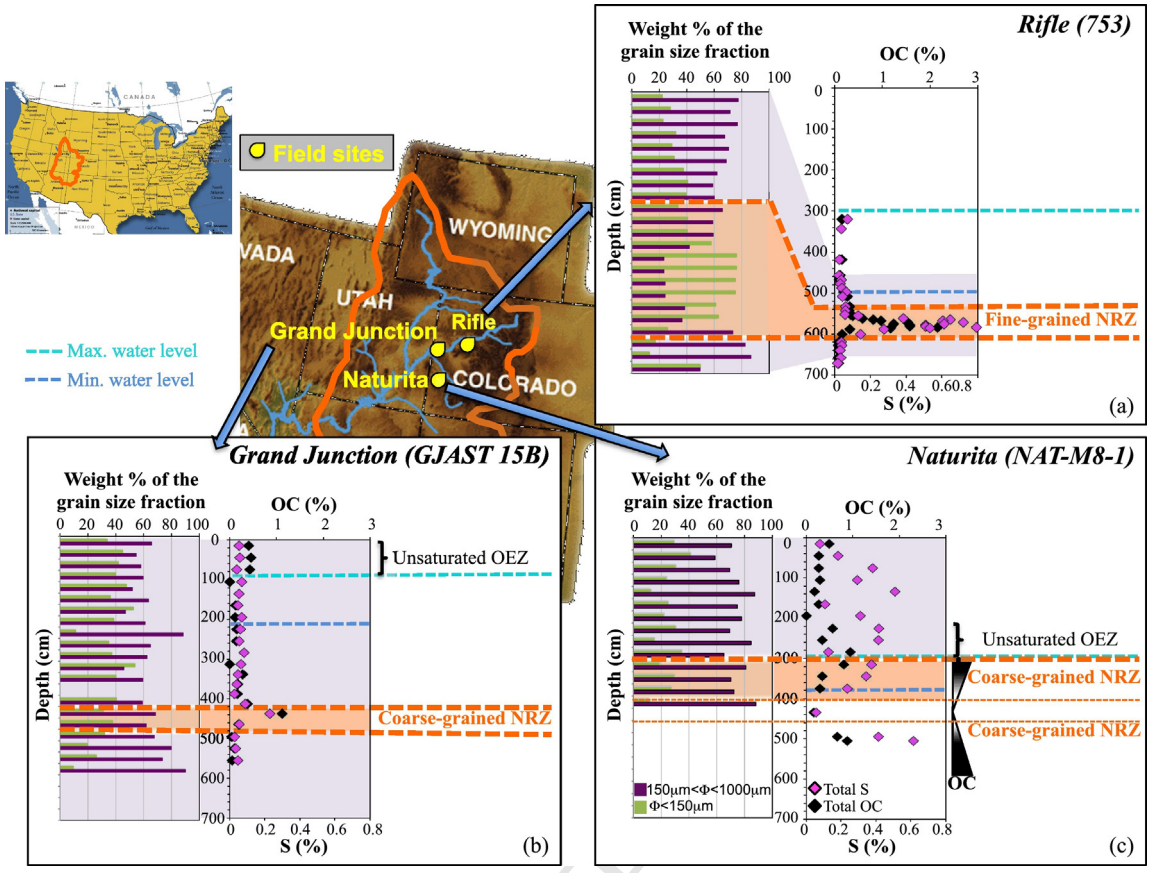

Fig. 1. Map of the Upper Colorado River Basin showing the location of the three field sites: (a) Rifle, (b) Grand Junction and (c) Naturita, CO. Profiles (left) show the distributions of particles between 1000 μm and 150 μm diameter (purple) and the particles <150 μm (green). Composition profiles (right) show bulk sediment total organic carbon (OC, black) and total sulfur (S, pink) concentrations. Blue dotted lines show the minimum (Min.) and maximum (Max.) levels of groundwater table; Orange dotted lines and shading show the location of the fine- and coarse-grained NRZs. For Naturita (c), additional vertical graphs on far right-hand side give abundances of key OC described in text (§3.1). Unsaturated OEZ = OEZ permanently located above the water table level; Fine-grained NRZ = NRZ enriched in fine particles (<150 μm) compared to surrounding sediments; Coarse-grained NRZ = NRZ with same distribution of grain sizes as surrounding sediments (cf., Table 1). Images from http://aspenjournalism.org/2014/03/30/snowpack-and-runoff-potential-looking-good/ and http://www.nationsonline.org/oneworld/usa_map.htm. (For interpretation of the references to color in this figure legend, the reader is referred to the web version of this article.)

sieved in order to get the <1 mm size fraction. Then the samples were homogenized and stored in sealed containers in an anoxic glove box.

2.2. Chemical analyses

Bulk sediments were ground and a 3 g sub-sample of powdered sediments was analyzed for total chemical compositions using X-ray fluorescence spectrometry with a SPECTRO XEPOS energy dispersive X-ray fluorescence spectrometer equipped with a Pd cathode and operating at 50 kV and 40 mA at the Stanford Environmental Measurements Facility. Each concentration was an average of 3 analyses quantify by a supplier-provided software and the *NIST 2711* certified reference material was intercalated during the analytical series. Organic C content was determined on a 200 mg sub-sample where carbonate C had been removed by adding aliquots of 1 mL 1 M HCl for >1 h until effervescence was undetectable. The remaining solution was decanted, sediments were dried at 30 °C and homogeneously mixed prior to analysis with a Carlo Erba NA1500 elemental analyzer. Subsets of select samples were dried and ~100 g of the <1 mm fraction was sieved into 4 fractions using a standard series of mesh sizes. Size fractions were separated by sieving bulk samples using a set of 3″ stainless steel and brass-nested sieves (53 μm, 150 μm, 500 μm, 1000 μm) by hand shaking. Additional details of analytical procedures are reported in the Appendix A.

2.3. Mössbauer spectroscopy

Fe-rich minerals compositions of bulk ground samples were analyzed by Mössbauer spectroscopy. Mössbauer spectra were collected using a Web Research Company (St. Paul, MN) instrument that included a closed-cycle cryostat SHI-850 obtained from Janis Research Company, Inc. (Wilmington, MA), a Sumitomo CKW-21 He compressor unit, and a Ritverc (St. Petersburg, Russia) NaI detection system. 57Co/Rh source (75-mCi, initial strength) was used as the gamma energy source. The raw data was folded to 512 channels to provide a flat background and a zero-velocity position corresponding to the center shift (CS) of a metal Fe foil at room temperature (RT). Calibration spectra were obtained with a 25-μm-thick Fe foil (Amersham, England) placed in the same position as the samples to minimize any geometry errors. The Mössbauer data were modelled with RecoilTM software (University of Ottawa, Canada) using a Voigt-based structural fitting routine (Rancourt and Ping, 1991). Sample preparation and sample holder were identical to the procedures reported in Peretyazhko et al. (2013).

2.4. X-ray absorption spectroscopy (XAS) data collection

Fluorescence-yield X-ray Absorption Near Edge Structure (XANES) K-edge spectra of S from the bulk ground sediment samples were

measured at beamline 4–3 at the Stanford Synchrotron Radiation Lightsource (SSRL), using a Si (111) double crystal monochromator. Samples were pressed into Al holders and covered with S-free plastic x-ray windows (4 μm thick 'parylene') inside a glove box (5%H_2/95%N_2 atmosphere). Spectra were collected under He atmosphere at room temperature in fluorescence mode using a SiLi Vortex detector. The X-ray energy was calibrated to the K-edge of sodium thiosulfate (2472 eV). Each XANES spectrum was composed of an average of 6 scans. No beam damage was detected and self-absorption was considered to be insignificant since most samples are fine-grained with S-concentrations <2% (Prietzel et al., 2011).

Fe K-edge XANES and X-ray Absorption Fine Structure (EXAFS) spectra of sediment samples were collected in fluorescence mode at 10 K on the 4–1 beamline at SSRL using a Si(220) double crystal monochromator. Bulk ground sediment samples were mounted on the cryostat sample rod within an N_2-purged glove bag and brought to the beamline in a liquid nitrogen bath before being rapidly transferred into the liquid He cryostat. The energy was calibrated by setting the first K-edge inflection point of a Fe foil to 7112 eV (double transmission mode). For each sediment sample, 3 to 12 scans were recorded, depending on the concentration (1.4 to 3.5 wt% Fe) and speciation of Fe.

S and Fe K-edge spectra were averaged and normalized using the ATHENA software (Ravel and Newville, 2005). S K-edge XANES data were analyzed by linear combination-least squares (LC-LS) fitting using reference spectra and S characteristic resonances from species observed in μ-XANES studies (described in Appendix A; Fig. S2). The Fe K-edge XANES and EXAFS spectra were fitted by a LC-LS fitting procedure using the ATHENA software, and using a homemade software based on Levenberg–Marquardt minimization algorithm (Hohmann et al., 2011; Pantke et al., 2012), respectively. Radial distribution functions around the Fe absorber were obtained by Fast-Fourier-transformation of the k^3-weighted experimental χ(k) function using a Kaiser-Bessel apodization window with the Bessel weight fixed at 2.5. Spectra were then analyzed by LC-LS fitting using the model compounds spectra selected from S K-edge XANES data analyses combined with mineralogical analysis given by Mössbauer results. Details of LC-LS fitting procedure are reported in the Appendix A. Experimental S and Fe K-edge XANES and EXAFS spectra from natural and synthetic model compounds used for LC-LS fitting analysis of XAS spectra of the sample sediments are described in the Appendix A.

3. Results

3.1. Sediment characterization

Vertical profiles of OC (organic carbon), total S, and particle size distribution within collected cores from Rifle, Grand Junction and Naturita are shown in Fig. 1. We identified horizons in all cores with an OC content that was markedly higher compared to the majority of the core sediment, i.e. sediments with C content two- to three-fold (minimum) higher than the surrounding sediments of studied basin. These were selected as candidate sediment zones adhering to the 'Rifle model' and were termed *organic-enriched zones* (OEZ). Based on their texture and position relative to the water table they were further divided into three subcategories (Table 1):

Unsaturated OEZ. OEZ located between the surface and the groundwater table. Such zones are found between 0 and ~90 cm depth below ground surface (bgs) in the core from Grand Junction (GJAST15B core, Fig. 1b) and at between 270 and 300 cm depth bgs in the core from Naturita (NAT-M8-1 core, Fig. 1c).

Saturated fine-grained OEZ. OEZ located below the groundwater table with a higher abundance of fine particles than the bulk average (e.g. Rifle core 753,300 cm bgs; Fig. 1a; Table 2). In both Rifle cores, OC concentrations increased up to seven-fold from an average of 0.15 wt% to average of 0.62 and 1.12 wt%, between 488 and 520 cm bgs in the 748 core, and between 555 and 588 cm bgs in the 753 core. These OEZ consisted of black clayey, centimeter-thick layers infilling interstices created by cobbles. At Rifle, the OEZ were easily distinguished from the surrounding alluvium, which was composed of oblate, spheroidal siliciclastic cobbles larger than 5 cm in diameter, pebbles, gravel, and sand exhibiting a light brown color (Janot et al., 2016). Indeed, sieving confirmed a higher abundance of fine particles (<150 μm) in the OEZ in Rifle core 753, specifically from 572 cm bgs (70% of the <1000 μm fraction), than in the rest of the core (32% of the <1000 μm fraction; Fig. 1a).

Table 1
Terminology used in this manuscript to describe the different type of sediments horizons in the upper Colorado River Basin (UCRB).

Terminology	Characteristics of sediment	The primary sulfide minerals
Organic-enriched sediments (OEZ)	Sediments with organic C content two- to three-fold (minimum) higher than the surrounding sediments	
Naturally reduced zones (NRZs)	OEZ containing reduced forms of sulfur S(-I), and/or S(-II) = *saturated OEZ; localised below the groundwater table at collecting date*	
Fine-grained NRZs ('Rifle' model)	NRZ with fine particles (<150 μm) content more abundant than in the surrounding sediments = *saturated fine-grained OEZ*	Mackinawite (FeS) Pyrite (FeS_2) Elemental sulfur
Coarse-grained NRZs 'Grand Junction and Naturita' model	NRZ with same distribution of grain sizes (within the <1000 μm fraction) as the under- and overlying aquifer sediments = *saturated coarse-grained OEZ*	Pyrite (FeS_2) Elemental sulfur

Saturated coarse-grained OEZ. OEZ located below the groundwater table with a texture similar to the remainder of the profile, i.e. where the OC content is the main distinguishing feature of the OEZ relative to the rest of the core. For example, the GJAST15B core (Grand Junction) contained an OEZ at 438 cm bgs distinguished by an increase in OC from an average of 0.20 wt% to 1.12 wt% (Fig. 1b), but the color and texture (dark grey clayey sand) are overall similar to the surrounding material (dark greyish brown sand). Similarly, in the NAT-M8-1 core (Naturita) the OC concentrations decreased from 0.81 wt% to 0.16 wt% between 315 and 435 cm bgs, then increased again to 0.78 wt% between 495 and 515 cm bgs (Fig. 1c). Otherwise this OEZ appeared to be similar to the surrounding brown clayey sand. Therefore, in contrast to the OEZ found at Rifle, it was more difficult to visually identify OEZ at Grand Junction and Naturita. Indeed, there was no distinct difference in the grain size distribution between OEZ and surrounding sediments in the GJAST15B and NAT-M8-1 samples, and coarse particles (>150 μm) were abundant (70% of the <1000 μm fraction) in the OEZ of Grand Junction and Naturita (Fig. 1b,c).

3.2. Total sulfur and total iron profiles

Total sulfur and total iron in core samples are given in Table 2. Total sulfur profiles are shown in Fig. 1. Below the water level (in the aquifer sediments), the saturated fine-grained and coarse-grained OEZ are enriched in S compared to aquifer sediments. Total S increased 10-fold at Rifle, from 0.05 wt% in the aquifer sediments to 0.61 and 0.52 wt%, in the OEZ of 748 and 753 cores, and 2-fold at Grand Junction, from 0.05 wt% in the aquifer sediments to 0.12 wt%, in the OEZ of GJAST15B core. At Naturita, the trends in total S and total OC were concomitant: total S decreased from 0.37 wt% to 0.06 wt% between 315 cm and 435 cm, and increased up to 0.61 wt% between 495 and 505 cm. Below the water table, the saturated fine- and coarse-grained OEZs are also slightly enriched in Fe compared to aquifer sediments. For example, at Rifle, total Fe increased from 1.86–2.11% in the background aquifer

Please cite this article as: Noël, V., et al., Understanding controls on redox processes in floodplain sediments of the Upper Colorado River Basin, Sci Total Environ (2017), http://dx.doi.org/10.1016/j.scitotenv.2017.01.109

Table 2
Table of chemical values (OC, S, Fe) for the different samples of the 4 cores. Blank cells correspond to undetermined data.

Rifle - 748 core			
Depth (cm)	OC (%)	S (%)	Fe (%)
244	0.25	0.03	1.89
282	0.21	0.03	2.22
325	0.14	0.04	2.45
363	0.15	0.04	1.86
393	0.20	0.06	2.47
445	0.29	0.06	2.16
461	0.21	0.05	2.07
471	0.15	0.05	1.92
480	0.17	0.06	2.07
488	0.57	0.42	2.51
492	0.85	0.58	2.77
497	0.71	0.72	2.79
503	0.66	0.65	2.60
520		0.68	2.51
544	0.20	0.10	2.47
565	0.16	0.08	2.43
585	0.15	0.09	2.26
613	0.16	0.04	1.93
652	0.15	0.07	2.02
705	0.15	0.07	2.07
743	0.12	0.04	2.19
781	0.12	0.04	2.28
819		0.02	2.21
887		0.06	1.42
933	0.11	0.06	1.71

Rifle - 753 core			
Depth (cm)	OC (%)	S (%)	Fe (%)
320	0.15	0.07	2.69
343	0.15	0.04	2.15
419	0.15	0.03	2.14
457	0.11	0.02	1.62
467	0.09	0.04	1.83
477	0.11	0.03	1.87
488	0.15	0.04	2.15
498	0.20	0.06	2.09
508	0.27	0.04	2.06
533	0.31	0.06	2.39
543	0.30	0.06	2.18
552	0.34	0.06	2.18
555	0.38	0.13	2.31
562	0.58	0.38	2.53
565	0.81	0.65	3.01
568	0.97	0.61	3.19
572	1.52	0.72	3.54
575	1.24	0.61	3.20
578	1.57	0.51	2.90
581	1.58	0.51	2.97
584	2.15	0.80	3.29
585	1.17	0.53	3.03
588	0.32	0.28	2.87
600	0.15	0.14	2.06
619	0.09	0.04	1.70
628	0.08	0.04	1.42
640	0.07	0.03	1.52
658	0.08	0.03	1.65
671	0.08	0.02	1.50
747	0.09	0.02	1.34
800	0.08	0.02	1.54
876	0.10	0.03	1.69
930	0.11	0.03	1.65
953	0.11	0.03	1.45

Grand Junction - GAST15B core			
Depth (cm)	OC (%)	S (%)	Fe (%)
15	0.40	0.05	1.87
45	0.46	0.06	2.63
75	0.43	0.04	3.37
105	0.24	0.07	3.05
135		0.05	2.40
165	0.13	0.05	2.56

Table 2 (*continued*)

Grand Junction - GAST15B core			
Depth (cm)	OC (%)	S (%)	Fe (%)
195	0.11	0.07	3.15
225	0.15	0.06	2.94
255	0.14	0.05	2.45
285		0.08	2.81
313	0.23	0.06	2.21
338	0.28	0.05	2.58
363	0.18	0.04	1.94
388	0.17	0.03	1.85
413	0.38	0.09	2.33
438	1.12	0.23	2.90
463	0.19	0.05	2.15
495	0.04	0.03	2.26
525	0.10	0.03	2.57
555	0.05	0.05	2.61

Naturita - NAT-M8-1 core			
Depth (cm)	OC (%)	S (%)	Fe (%)
15	0.49	0.08	2.12
45	0.27	0.18	2.29
75	0.27	0.38	2.20
105	0.29	0.29	2.23
135	0.18	0.51	2.66
165	0.27	0.11	2.85
195	0.41	0.31	2.42
225	0.57	0.42	2.32
255	0.34	0.41	2.00
285	0.95	0.13	2.64
315	0.81	0.37	1.84
345	0.34	0.34	1.92
375	0.29	0.24	1.91
435	0.16	0.06	1.53
495	0.67	0.41	1.67
505	0.88	0.61	1.89

sediments to maximums of 2.64 and 2.99% in 748 and 753 cores, respectively.

3.3. Sediment redox conditions: fine-grained NRZ vs. coarse-grained NRZ

Vertical profiles of S oxidation state within collected cores from Rifle, Grand Junction and Naturita are shown in Fig. 2. S K-edge XANES spectra show a strong reduction in S oxidation state in saturated OEZs as compared to surrounding sediments (Figs. 2, 3a and S3, S4). The saturated OEZs are characterized by Fe(III) and sulfate-reducing products (Figs. 2, 3 and 5), and are consequently referred to as 'naturally reduce zones', NRZs (Campbell et al., 2012). Based on their texture, saturated OEZ were divided into two subcategories (detailed in §3.1, Table 1, and Fig. 1): (1) 'fine-grained NRZs', such as those observed at the Rifle site; and (2) 'coarse-grained NRZs', such as those observed at the Naturita and Grand Junction sites. The NRZ sediments at Grand Junction and Naturita exhibit the same grain size distribution (within the <1000 μm fraction) as the under- and overlying aquifer sediments. These NRZs are coarser-grained than those at Rifle. S K-edge XANES spectroscopy provides a redox indicator for sulfur and is an efficient technique for characterizing S oxidation state and iron sulfide species in complex natural materials (Fleet, 2005). Based on the K-edge XANES, the two subcategories of NRZs show different S oxidation states and, consequently, different iron sulfides:

Fine-grained NRZs. S XANES spectra of the fine-grained NRZ from Rifle show the occurrence of S(VI), S(0), S(-I), and S(-II), as identified by the energy position of absorption-edge peaks (1s-3p) at 2482.6 eV, 2472.4 eV, 2472 eV and 2470.9–2470.3 eV, respectively (Figs. 2, 3 and S3). The peak at 2470.9–2470.3 eV was previously interpreted as the concomitant occurrence of mackinawite (FeS) and greigite (Fe_3S_4) (Janot et al., 2016). However in a subsequent study, we have found

Please cite this article as: Noël, V., et al., Understanding controls on redox processes in floodplain sediments of the Upper Colorado River Basin, Sci Total Environ (2017), http://dx.doi.org/10.1016/j.scitotenv.2017.01.109

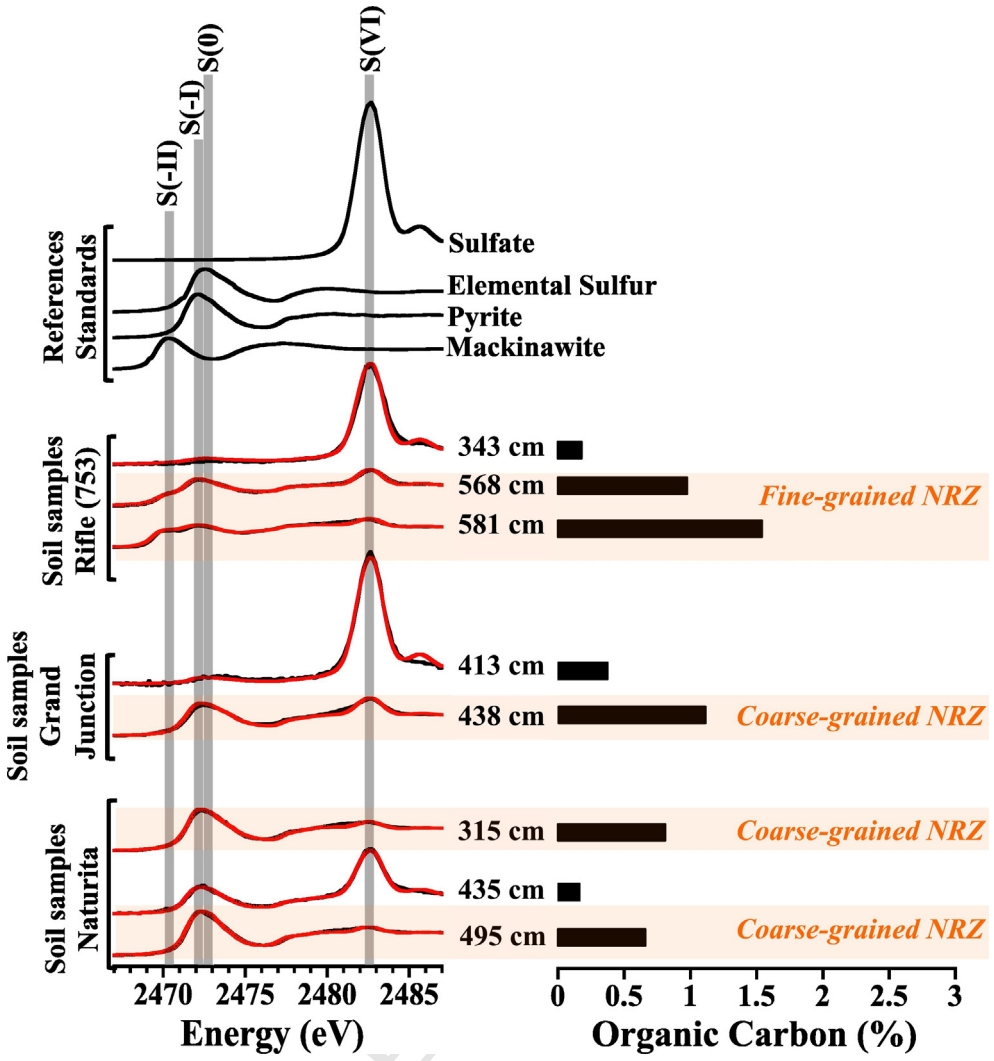

Fig. 2. Representative bulk S K-edge XANES spectra (left) of water saturated sediments as function of organic carbon concentration (right). The selected spectra are representative of S speciation evolution for cores from Rifle, Grand Junction and Naturita; all of bulk S K-edge XANES spectra of sediment samples collected along the cores from Rifle and from Grand Junction and Naturita are shown Fig. S3 and S4, respectively. Orange shading shows the location of the NRZs. Red lines are fits to spectra. Sample spectra are compared to reference spectra (top) for: mackinawite, pyrite, elemental sulfur and sulfate. Thick vertical grey bands denote characteristic 1s-3p resonances for each oxidation state. Depths below ground surface (bgs) are noted numerically. (For interpretation of the references to color in this figure legend, the reader is referred to the web version of this article.)

that synthetic FeS exposed to sub-stoichiometric amounts of oxidants or Fe^{3+} exhibits a peak at 2470.3 eV (Fig. S2). This FeS phase, referred to as minimally oxidized mackinawite, shows a peak shift in S XANES up to −0.6 eV compared to theoretical mackinawite. The S K-edge XANES peak at 2470.3 eV, characteristic of S(-II), is thus interpreted as the occurrence of mackinawite with partial degrees of oxidation but retaining most of the characteristics of FeS. Mössbauer data does not show any indication of greigite (Fig. 4c). Therefore the occurrence of greigite in fine-grained NRZ from Rifle is considered unlikely.

Coarse-grained NRZs. In contrast to the Rifle samples, only three oxidation states of sulfur were distinguished in the samples collected in the coarse-grained NRZs of Grand Junction and Naturita (Fig. 2 and S4). The S K-edge XANES peaks at 2482.6 eV and 2472.4 eV were interpreted as sulfate and elemental sulfur, respectively. The peak at 2472 eV was attributed to pyrite, as suggested by the Mössbauer spectroscopy results (Fig. 4c). In these coarse-grained NRZs, no iron monosulfide phases were detected by S K-edge XANES analysis.

3.4. Detailed Fe speciation in the NRZs

The Fe mineral composition of the fine-grained Rifle NRZ (753 core, 568 cm bgs) and the coarse-grained Grand Junction NRZ (GJAST15B core, 438 cm bgs) are shown in Fig. 4a,b. In both cases, a considerable fraction of the total Fe is unambiguously present as crystalline/large-particle hematite and magnetite (sextet features in the modelled spectra), and as Fe(II) in phyllosilicates (red doublet in Fig. 4a,b). The remaining Fe displayed as a quadrupole splitting. Around 0 to +2 mm/s (blue doublet in Fig. 4a,b) is undoubtedly a mix of phyllosilicate Fe(III) and diamagnetic Fe(II)-sulfides, pyrite and/or mackinawite (for additional details about Mössbauer spectra analyses, see Supplementary data). Goethite and ferrihydrite are not evidence in the RT, 140 K, and 77 K spectra, and 77 K and 8.5 K. The absence of these phases is consistent with the anoxic nature of NRZs, since these bioavailable Fe-oxide phases are present in Rifle background sediments (Campbell et al., 2012). Furthermore, it is clear from Mössbauer spectra that stronger anoxic conditions prevail in the Rifle NRZ than in the Grand Junction NRZ, based on the relative contribution of phyllosilicate Fe(II) to the spectra, since phyllosilicate Fe(II) content has been shown to increase as a result of bioreduction (Kukkadapu et al., 2006). Finally, Fig. 4c clearly shows that greigite was not present in the samples.

The Mössbauer results were in agreement with the LC-LS results of the XAS data (Fig. 4d). Hematite, magnetite, and Fe(II)- and Fe(III)-phyllosilicates were previously described at Rifle, both in the NRZ and surrounding sediments. These minerals were mainly inherited from

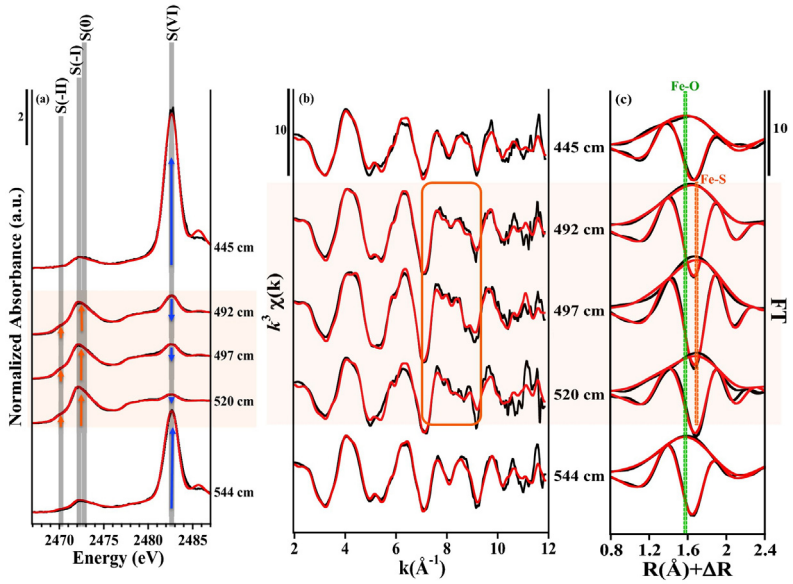

Fig. 3. (a) S K-edge XANES of the Rifle (748 core) sediments as a function of depth in comparison to (b) Fe K-edge EXAFS spectra (black lines) and LC-LS fitting curves (red lines) and (c) their corresponding Fourier Transforms. Orange shading shows the location of the fine-grained NRZ and the orange box highlights the spectral characteristic changes of Fe K-edge EXAFS around k = 8 Å^{-1}. Depths below ground surface (bgs) are noted numerically. (For interpretation of the references to color in this figure legend, the reader is referred to the web version of this article.)

burial of sediments along active river margins (Qafoku et al., 2009; Campbell et al., 2012). Thus, it is reasonable to find similar Fe-bearing phases in alluvial floodplains at other sites (Grand Junction and Naturita; Fig. 5 and Table S2) in the UCRB. Fe K-edge EXAFS spectra of illite, biotite and phlogopite provided the best fits to minimize the Rf of LC-LS fitting of soil samples. Illite and phlogopite were thus chosen as proxies for Fe(II–III)-phyllosilicates, (Karickhoff and Bailey, 1973; Johnston and Cardile, 1987) and biotite for Fe(II) phyllosilicates (Faye, 1968). Iron sulfides, such as pyrite, were previously described to occur in the NRZ (Janot et al., 2016). The model compounds used for the LC-LS fitting analyses are reported in Fig. S7.

Similarly to the Mössbauer data, Fe K-edge EXAFS spectra suggested stronger anoxic conditions in the Rifle NRZ than in the Grand Junction NRZ. Pyrite was detected in the sediment of the Rifle NRZ (753 and 748 cores; Fig. S8 and Table S2), whereas it was not detected in the sediments of the Grand Junction NRZ (GJAST15B core; Fig. S9 and Table S2). The absence of a species from Fe K-edge EXAFS suggests that its proportion is below 10% of the total Fe content (the detection limit of this method; Cancès et al., 2005; Juillot et al., 2011). However, the S K-edge XANES of Grand Junction NRZ sediment shows that pyrite is a major species when evaluated relative to the total S content (Fig. S4 and Table S1). A large fraction of pyrite also was detected by Fe speciation analyses of the coarse-grained NRZ collected at Naturita (NAT-M8-1 core) (Fig. S9 and Table S2). This indicates sulfate-reducing conditions can also occur in the coarse-grained NRZs.

3.5. Vertical transects distributions and quantitative speciation of Fe and S species through floodplain alluvium

Results from speciation studies detailed in 3.3§ and 3.4§ were used as the basis for comprehensively and vertically profiling Fe/S species through an entire alluvium cross-section. LC-LS fitting of EXAFS and XANES spectra are shown in Fig. 5 and parameters are summarized in Table S1 and S2 for the S and Fe speciation, respectively.

Fine-grained NRZs. In the sediments collected at Rifle (example of 753 core detailed in Fig. 5a,b,c), Fe EXAFS data indicate that in the sediments collected above and below the NRZs, approximately half of Fe was present in phyllosilicate minerals, including Fe(II–III)-bearing phyllosilicates (43%) and, to a lesser extent Fe(III)-bearing phyllosilicates (12%). Fe(III)-oxyhydroxides and Fe(II-III)-oxides also comprised about half of total Fe. Fe(III)-oxyhydroxides (25%) included mainly hematite and goethite, whereas Fe(II–III)-oxides (21%) occur as magnetite. In the fine-grained NRZ, the proportion of goethite decreased from the interface with the surrounding aquifer (588 cm bgs), to undetectable amounts in the interior of the NRZ (562–568 cm bgs). Concomitantly, pyrite appeared as an additional Fe pool in the NRZ, with proportions increasing inversely to the goethite fraction, from 10% at 588 cm bgs to 17% at 568 cm bgs (Fig. 5c). The remaining fraction of Fe in the fine-grained Rifle NRZs was incorporated into phyllosilicate minerals (50%), magnetite (14%) and hematite (16%) in constant proportions throughout the NRZ. Similarly to Fe, the S speciation indicates increasing proportions of iron sulfides (FeS and FeS_2) from the interface with aquifer sediments (57% at 555 cm bgs and 38% at 619 cm bgs) to the interior of the NRZ (up to 90%) (Fig. 5b and S5). Concomitantly, the proportion of sulfate and elemental sulfur decreased from the interface to the interior of the NRZ. Detailed results of the LC-LS fitting normalized to 100% for the NRZ sediments from 748 and 753 cores are shown in Fig. S5.

Coarse-grained NRZs. The S XANES data (detailed in Fig. S4) from the saturated coarse-grained NRZs from Grand Junction and Naturita show occurrence of pyrite (24–44% and 27–70% of total sulfur, respectively) and relatively abundant elemental sulfur (38–48% and 15–41% of total sulfur, respectively (Fig. 5e,h). Unlike Rifle, these saturated coarse-grained NRZ do not show occurrence of iron monosulfides. Instead, relatively high proportions of elemental sulfur are present. In the sediments collected above and below the NRZs in these cores (GJAST15B and NAT-M8-1), Fe EXAFS data (detailed in Fig. S9) are characterized by high proportions of Fe(III)-bearing phyllosilicates such as illite (36–40%) and, to a lesser extent Fe(II–III)-bearing phyllosilicates, such as phlogopite (16–17%). The second half of the Fe fraction is present as Fe(II–III)-oxides, as magnetite (26 and 12% for GJAST15B and NATM8-1, respectively), and Fe(III)-oxyhydroxides, including hematite and goethite (22 and 30% for GJAST15B and NATM8-1, respectively) (Fig. 5f,i). However, the goethite pool was not apparent in the Grand Junction coarse-grained NRZ, which was confirmed by Mössbauer analysis (438 cm bgs sample) (Fig. 4). At Grand Junction, iron sulfides were below detection (~10%) in the Fe pool (Fig. 5f). In the NAT-M8-1 core from Naturita, goethite was not seen in the NRZ samples richer in OC (315 and 505 cm bgs) below the water table. In these sediments,

Please cite this article as: Noël, V., et al., Understanding controls on redox processes in floodplain sediments of the Upper Colorado River Basin, Sci Total Environ (2017), http://dx.doi.org/10.1016/j.scitotenv.2017.01.109

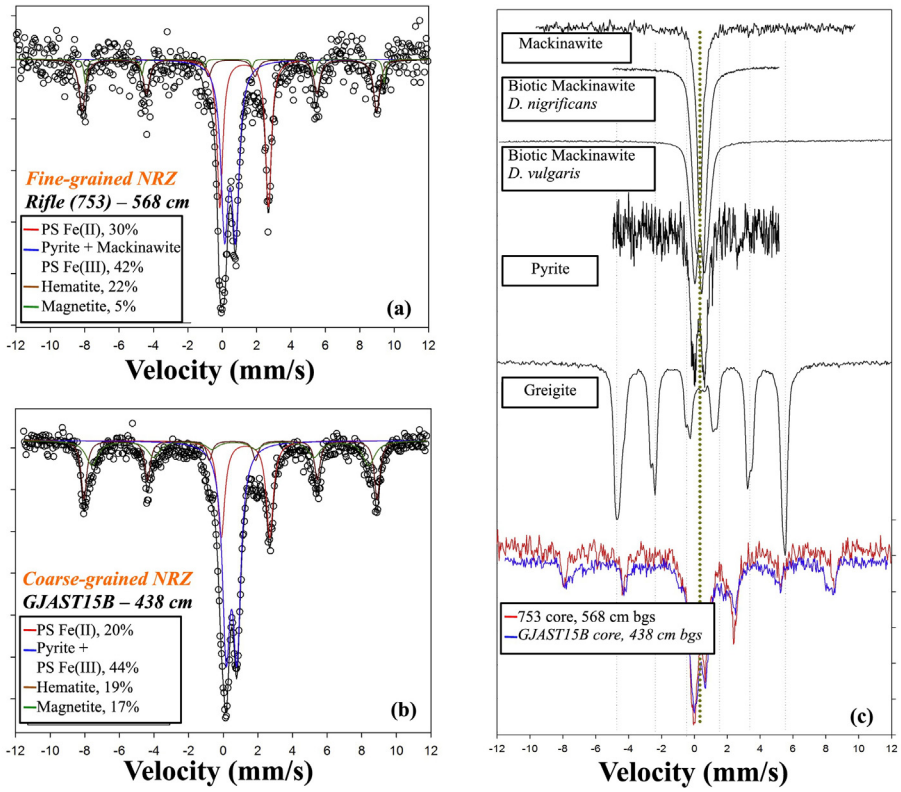

(d)	Rifle (753) 568 cm bgs			GJAST15B 438 cm bgs		
	Mössbauer	EXAFS	*Occurence from S K-edge XANES*	Mössbauer	EXAFS	*Occurence from S K-edge XANES*
% Fe(II)-Clays	30	32		20	23	
% Fe(III)-Clays		21			44	
% Fe-Pyrite	42	17	+	44	Below the detection limit	+
% Fe-Mackinawite		Below the detection limit	+		Below the detection limit	-
% Fe-Hematite	22	19		19	15	
% Fe-Magnetite	5	10		17	19	

Fig. 4. Liquid nitrogen (77 K) modelled Mössbauer spectra of (a) fine-grained Rifle NRZ (753 core; 568 bgs), (b) coarse-grained Grand Junction NRZ (GJAST15B: 438 cm bgs), (c) comparison of RT Mössbauer spectra of NRZs to Fe-sulfide standards, and (d) comparison of relative proportions of Fe-species from Mössbauer spectroscopy with LC-LS fitting of Fe Kedge EXAFS. PS: phyllosilicates. The occurrence of iron sulfides from quantitative study of S K-edge XANES (Fig. 5) is reported for each phase below the detection limit of LC-LS fitting of Fe K-edge EXAFS (estimated to 10%); with (−) not observed, and, (+) observed as major phase, respectively.

however, pyrite was present (15–24%), and increased with organic carbon concentration (Fig. 5i). Similar to Fe, the S speciation indicated an increased proportion of pyrite, proportional to the organic carbon content (Fig. 5h). As in the samples collected in the fine-grained NRZ of Rifle, the remaining fraction of Fe in coarse-grained NRZs was incorporated in phyllosilicate minerals, magnetite and hematite.

4. Discussion

4.1. Regional significance of NRZs

Janot et al. (2016) proposed that NRZs should be present in alluvial floodplains throughout the UCRB, and that Rifle NRZs provide a model for biogeochemical behavior of floodplains regionally. Three conditions were proposed to be critical to the development of NRZs: (i) saturation of pore space by water, (ii) enhanced organic matter content, and (iii) fine sediment grain size (Campbell et al., 2012; Janot et al., 2016). The results of the present study support the hypothesis that NRZs are common features of alluvial floodplains throughout the UCRB and that pore saturation and elevated OC content are necessary properties for the development of NRZs (Fig. 6). However, our data reveal that fine-grained texture is not required to establish Fe(III) and sulfate reducing conditions (Fig. 5). Thus, we propose a modification of the 'Rifle model' of NRZs where the texture is of secondary importance relative to the OC content and water saturation for the establishment of NRZs, both of which have primary controls on oxygen delivery and consumption. Exchange of oxidants between NRZs and groundwater depends on the permeability of the NRZs, which is related to sediment texture. We therefore reason that the exchange of solutes and inflow of oxidants is relatively slow in diffusion-limited fine-grained NRZs. This renders the biogeochemical conditions in fine-grained NRZs comparatively stable relative to coarse-grained NRZs. In other words, NRZs can develop independent of texture as long as the OC content is high enough (0.7% total OC minimum; Table 2) and sediments are water saturated, but the NRZ sensitivity to oxidation is dependent on the texture. Thus, predictions of NRZ behavior in response to perturbations, such as

Please cite this article as: Noël, V., et al., Understanding controls on redox processes in floodplain sediments of the Upper Colorado River Basin, Sci Total Environ (2017), http://dx.doi.org/10.1016/j.scitotenv.2017.01.109

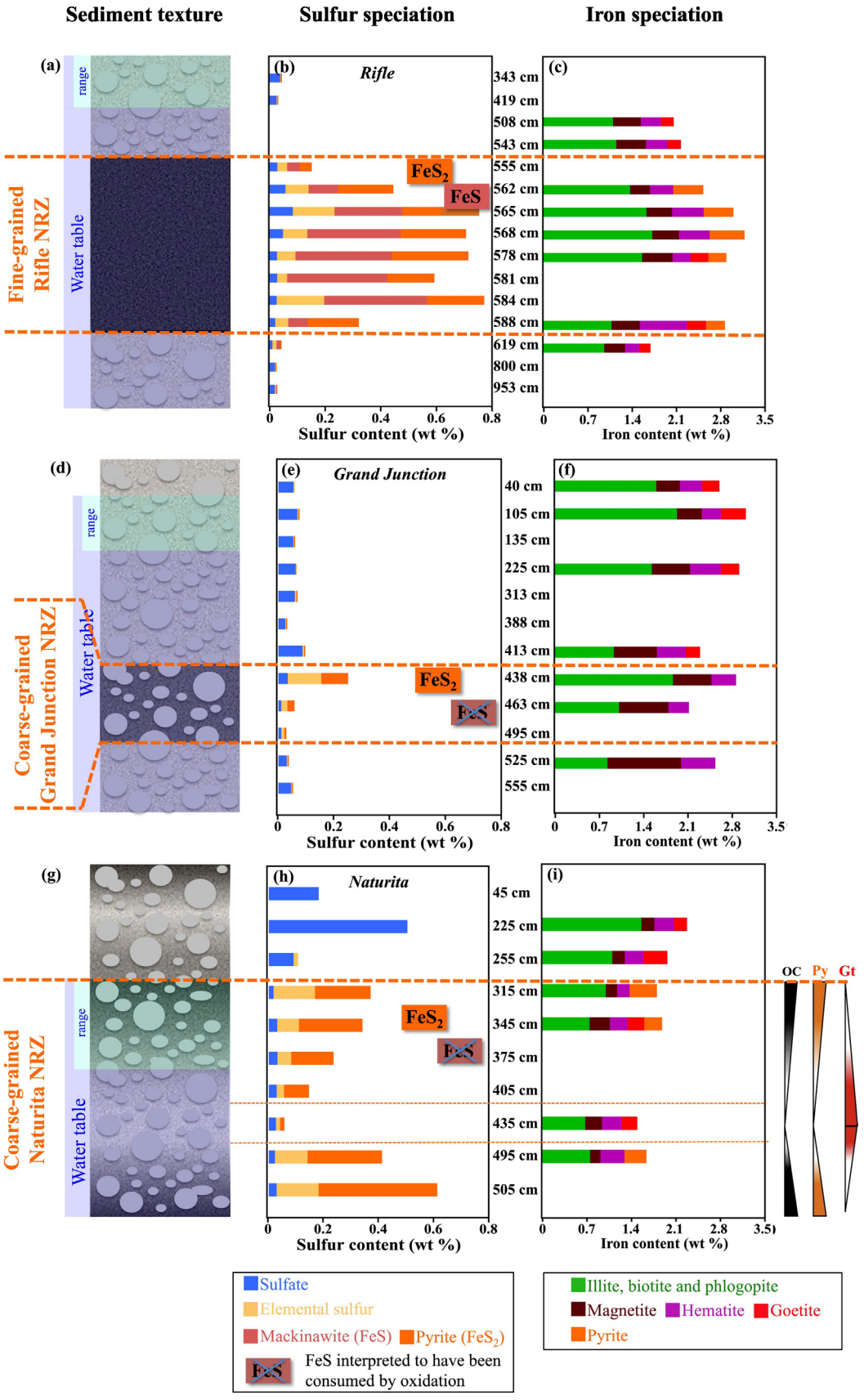

Fig. 5. S and Fe speciation in the bulk sediment samples from Rifle (top; 753 core), Grand Junction (middle; GJAST15B core) and Naturita (bottom; NAT-M8-1 core), as function of depth. For each site, the left-hand schema summarizes the sediment texture, organic carbon content, and saturation state (a,d,g). The bar plots show the quantitative speciation results of S (middle) and Fe (right) obtained from LC-LS fitting analysis of XANES and EXAFS, respectively. S-species (b,e,h) and Fe-species (c,f,i) are expressed as mass concentration (wt% S or Fe). The proportion of Fe-bearing phyllosilicates pools are detailed in Table SI-2. Depths below ground surface (bgs) are noted numerically. Bottom row: additional vertical graphs on far right-hand side give abundances of key components of organic carbon (OC), pyrite (Py) and goethite (Gt) described in text (Section 3.5).

Please cite this article as: Noël, V., et al., Understanding controls on redox processes in floodplain sediments of the Upper Colorado River Basin, Sci Total Environ (2017), http://dx.doi.org/10.1016/j.scitotenv.2017.01.109

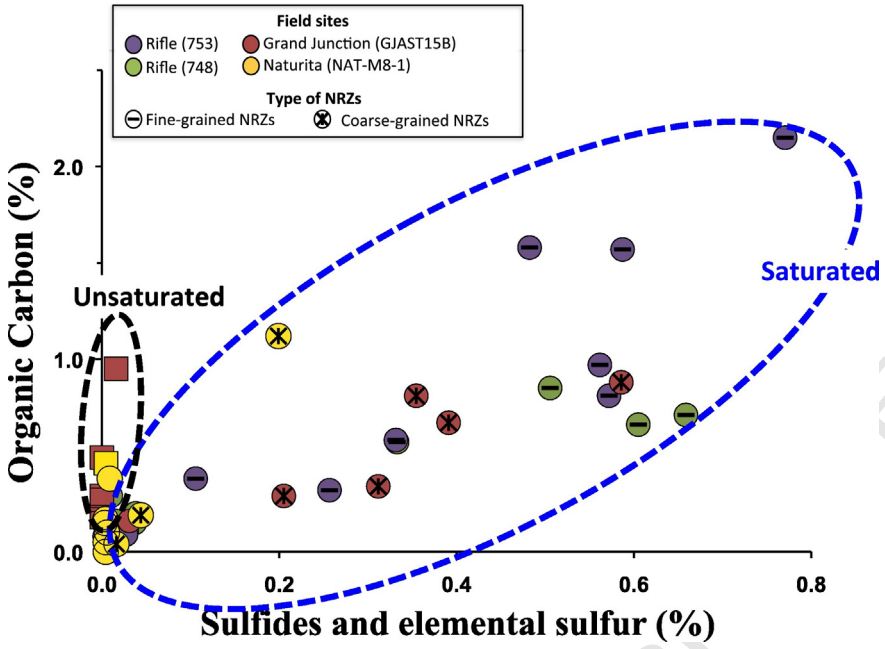

Fig. 6. Summary of distribution of elemental abundances of organic carbon and total reduced sulfur (sulfides and elemental sulfur) in all lithologic horizons (OEZ and surrounding sediments) from all samples at all sites: Rifle 753 (purple) and 748 (green); Grand Junction GJAST15B (red); and Naturita NAT-M8-1 (yellow). Square symbols: unsaturated sediments; Circle symbols: saturated sediments; Minus symbols: fine-grained NRZs; Cross symbols: coarse-grained NRZs. (For interpretation of the references to color in this figure legend, the reader is referred to the web version of this article.)

water table fluctuations, need to consider texture and permeability in addition to the OC content.

4.2. Redox behavior of NRZs

Sulfur and iron speciation are highly sensitive to the redox status within sediments and, thus, provide valuable information about processes affecting elemental cycling and the behavior of redox-active contaminants. In the current study, all NRZs exhibit a major change in the oxidation state of S from sulfates as the dominant solid-phase species in oxic sediments to sulfides inside NRZs (Fig. 5). The evolution of S species mirrors a shift in redox conditions from oxidizing to reducing conditions. Here we discuss process models for S and Fe transformations inferred from the results.

Reduction processes. S K-edge XANES and Fe K-edge EXAFS show that goethite, which was abundant in over-/underlying sediments, decreased concurrently with the appearance of iron sulfides in all NRZs observed here (Fig. 5 and Table S2). This observation suggests that iron sulfide precipitation is mechanistically linked to dissolution of goethite (Fig. 5, S4 and S9). Fe(III)-oxyhydroxide reductive dissolution can be driven by direct reduction of Fe^{3+} by metal-reducing heterotrophic bacteria, coupled to oxidation of organic carbon, in which case the primary products are CO_2 and Fe^{2+} (Nielsen and Andersen, 2003; Canfield et al., 2005). Fe(III)-oxyhydroxides can also be reduced abiotically by when biogenic H_2S produced by sulfate bacterial respiration (Rickard, 1975; Pyzik and Sommer, 1981; Wei and Osseo-Asare, 1997; Williams et al., 2011; Druhan et al., 2014) reacts with H_2S and Fe(III)-oxyhydroxides to produce elemental sulfur (Eq. (1)) and nano-crystalline mackinawite (Eq. (2)) (Wei and Osseo-Asare, 1997).

$$2Fe^{3+} + HS^- = 2Fe^{2+} + S^0 + H^+ \quad (1)$$

$$Fe^{2+} + HS^- = FeS + H^+ \quad (2)$$

These two products, mackinawite (FeS), together with elemental sulfur (S0), co-occured in the fine-grained Rifle NRZ sediments (Fig. 5 and Table S1). The concomitance of these two products in these sediments, combined with the concomitant disappearance of goethite, suggests that Fe^{3+} reduction in NRZ sediments follows the abiotic pathway described by Eqs. (1) and (2). Indeed, Fe^{3+} reduction using the biotic pathway does not produce elemental sulfur, however we cannot exclude that some Fe(III) bacterial respiration occurs. This conclusion is consistent with previous studies (Campbell et al., 2012; Janot et al., 2016). Furthermore, the production of elemental sulfur and sulfides (Fig. 6), as well as reductive dissolution of Fe(III)-oxyhydroxide in the coarse-grained NRZs (Fig. 5i), is proportional to the organic carbon content of NRZs. Thus, the intensity of Fe(III) and sulfate reducing conditions in NRZ sediments seem be mainly controlled by organic carbon content.

Oxidation processes. Iron monosulfides (e.g. mackinawite) are not observed in the coarse-grained Rifle NRZs (Fig. 5b,e,h). In contrast, pyrite is observed in all NRZ sediments. The systematic presence of pyrite along with the co-occurrence of elemental sulfur provides strong evidence for mackinawite previously existing as an intermediate in the formation of pyrite in the coarse-grained NRZs. Indeed, even if pyrite formation can arguably occur via a number of pathways (involving H_2S, S(0), polysulfides, greigite, Fe^{2+} or even FeOOH), only two mechanisms of sedimentary pyrite formation are currently accepted (Eqs. (3) and (4)) and both occur through the conversion of FeS (Rickard, 1975; Luther, 1991; Rickard, 1997; Rickard and Luther, 1997; Butler and Rickard, 2000; Burton et al., 2011).

$$FeS + S_n^{2-} = FeS_2 + S_{(n-1)}^{2-} \quad (3)$$

$$FeS + H_2S = FeS_2 + H_2 \quad (4)$$

The relative absence of mackinawite in coarse-grained NRZ sediments implies that it had been consumed, for example by oxidation. Importantly, mackinawite oxidation produces elemental sulfur (Burton et al., 2009); at near-neutral pH, S(0) forms as an initial solid-phase product of mackinawite oxidation in the presence of O_2-bearing solutions (Eq. (5)).

$$FeS + 0.75\ O_2 + 0.5\ H_2O = S^0 + FeOOH \quad (5)$$

Please cite this article as: Noël, V., et al., Understanding controls on redox processes in floodplain sediments of the Upper Colorado River Basin, Sci Total Environ (2017), http://dx.doi.org/10.1016/j.scitotenv.2017.01.109

Thus, mackinawite oxidation increases the S(0) content (Schippers and Sand, 1999; Burton et al., 2006, 2009). Although oxidation of mackinawite also affects the mineralogy of Fe, the S speciation changes were appreciably more noticeable in the sediment S pool, which was dominated by sulfides. In comparison, the iron pool was dominated by phyllosilicates and oxides. Consequently, the change in Fe speciation was less noticeable, but consistent with the S results. The coarse-grained NRZs in this study uniformly exhibit higher proportions of elemental S (50% of total S) compared to fine-grained NRZs (<20% of total S) (Table S1). This observation, combined with the absence of iron monosulfides and the occurrence of pyrite, suggests that FeS had been oxidized by molecular oxygen in the coarse-grained NRZs (Fig. 5).

Redox cycling of NRZs. It is logical that the impact of oxidant diffusion is more extensive and pronounced in coarse-grained than in fine-grained NRZs, because coarse-grained sediments have greater porosity, enabling faster solute and gas exchange with the surrounding environment. Iron monosulfides that precipitate during (bio)reduction processes, such as mackinawite, are metastable and widely regarded as precursors to thermodynamically-favored pyrite in the presence of oxidants (Schoonen and Barnes, 1991; Wilkin and Barnes, 1996; Benning et al., 2000; Otero et al., 2005; Hunger and Benning, 2007). Thus, the overall picture that emerges from the Fe and S chemical speciation is that higher sediment permeability leads to overall higher sulfide oxidation rates, higher abundances of elemental sulfur, and lower abundances of mackinawite. This model is illustrated schematically in Fig. 7. Thus the distribution of mackinawite in the NRZs of floodplain sediments of UCRB is proposed as a consequence of oxidation rates depending on the sediment texture. In addition to the diffusion-limitations preventing oxidation, the fine-grained NRZs are also systematically more enriched in organic carbon (Fig. 6), which should contribute to the ability of these NRZs to maintain and re-establish reducing conditions. Thus, we reason that coarse-grained NRZs are regularly oxidized, whereas fine-grained NRZs exhibit persistent-Fe(III)-and sulfate reducing conditions.

4.3. Implications for biogeochemical function and contaminant mobility

The persistence of Fe(III)- and sulfate-reducing conditions directly impacts the ability of NRZs to retain redox-active contaminants, i.e., contaminants that can occur in different oxidation states within the pE-pH conditions of natural waters, including As, Se, Mo, and U. Coarse-grained NRZs with higher permeability will be subject to more frequent and rapid redox cycling and, hence, to more dynamic exchange of contaminants with surrounding aquifers. The suspected greater ability of fine-grained NRZs to maintain and revert to reducing conditions (i.e. greater resilience), further improves the ability of these NRZs to act as sinks of trace contaminants should they become subject to periodic disturbances, such as partial desiccation during long-term or seasonal drought.

Differences in reactivity of different iron sulfide minerals (e.g., FeS and FeS_2) towards redox-active contaminants further enhances the ability of NRZs to retain trace contaminants (Hua and Deng, 2008; Burton et al., 2011; Hyun et al., 2012; Veeramani et al., 2013). For example, mackinawite occurs as a reactive high surface-area nanoscale mineral that can precipitate metals such as Cd. In comparison, similar minerals (e.g., pyrite), have much greater sorption capacity (Parkman et al., 1999)(Kornicker and Morse, 1991; Morse and Arakaki, 1993). Thus, fine-grained and coarse-grained NRZs likely exhibit different metal attenuation mechanisms, leading to different extents and rates of metal retention and release.

V, Cr, Mn, As, Se, Mo and U are traces-metals of concern in floodplains at legacy ore processing sites across the UCRB. The concentrations of these elements measured in the sediments collected along the studied cores in this study from Rifle, Grand Junction and Naturita are shown in Supplementary data (Fig. S10). Redox-active contaminants that are less mobile in their reduced forms, such as U(IV) and Cr(III), are expected to accumulate in NRZs, as are elements that are sequestered in sulfides. Exposure of NRZs to oxidants such as O_2 and NO_3^- will likely drive release of sequestered radionuclides, and metals. Oxidative conditions can occur seasonally during summer dry conditions and during periods of long-term drought. Thus, NRZs are likely to be nexuses of biogeochemical activity driven by hydrological dynamics that likely have important effects on floodplain water quality.

5. Conclusion

This study compares vertical redox profiles of reduced organic-rich sediments from 3 floodplain sites spanning a 250 km transect of the central UCRB. Key attributes evaluated include Fe and S redox status, mineralogy, organic carbon content, and particle size. Comparison of similarities and differences in their properties leads to the following key findings:

1. NRZs are common in floodplains in the UCRB.
2. NRZ reducing conditions and sulfide production are linked primarily to organic carbon content (0.7% total OC minimum is required), as well as sediment moisture.
3. Sediment grain size indirectly controls the abundance of the reactive species mackinawite and elemental sulfur by mediating oxidant diffusion in NRZs. Coarse-grained textures allow greater exposure to

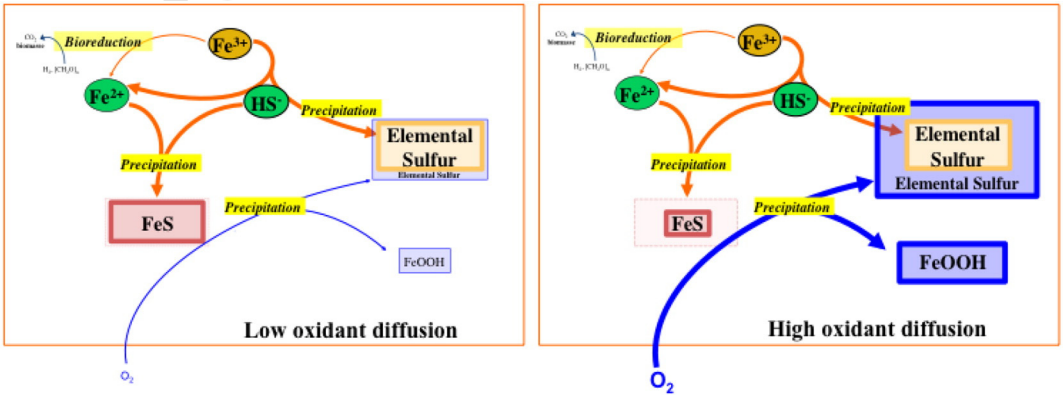

Fig. 7. Illustration of the biogeochemical reaction network believed to control abundances of iron monosulfides and elemental sulfur in NRZs. In this model, the primary oxidant is assumed to be O_2, which diffuses into NRZs (blue lines; thickness reflect abundance of oxidant) where it oxidizes FeS, leading to precipitation of S(0) and FeOOH. The overall rates and extents of these processes are proportional to sediment permeability. Inflow of oxidants is estimated to be relatively fast in coarse-grained NRZs but less important in fine-grained NRZs. Consequently, more elemental sulfur is produced and FeS is almost completely absent in coarse-grained NRZs. The maximum quantity of FeOOH produced by this reaction is estimated to be 3–4 wt%, which is below the 10% detection limit required to detect it by XAS in the pool of total iron. (For interpretation of the references to color in this figure legend, the reader is referred to the web version of this article.)

oxidants and conversion of mackinawite to elemental sulfur. In contrast, fine-grained sediments are enriched in mackinawite and deficient in elemental sulfur.

The ability of NRZs to accumulate heavy metals is due largely to (i) their low redox potentials, and (ii) the presence of the reactive elemental sulfur and mackinawite that can react with metals and precipitate as sulfides. NRZs are likely to play major roles in mediating contaminant behavior in floodplains where they reside.

Acknowledgments

Research was supported by the DOE-BER Climate and Environmental Sciences Division through the SLAC Science Focus Area (SFA) program and by DOE-BES through its support for SSRL. SSRL and SLAC are supported by the U.S. Department of Energy, Office of Science, Office of Basic Energy Sciences under Contract No. DE-AC02-76SF00515, the DOE Office of Biological and Environmental Research, and by the National Institutes of Health, National Institute of General Medical Sciences (including P41GM103393).

This material is partially based upon work supported through the Lawrence Berkeley National Laboratory's Genomes-to-Watershed Scientific Focus Area. The U.S. Department of Energy (DOE), Office of Science, Office of Biological and Environmental Research funded the work under contract DE-AC02-05CH11231 (Lawrence Berkeley National Laboratory; operated by the University of California).

We thank Craig Goodknight, Ray Johnson, Dick Dayvault, David Traub, Sam Campbell, David Miller, Sandy Beranich, David Atkinson, Dan Sellers, David Dander, Rob Rice, and Anthony Martinez of U.S. Department of Energy Office of Legacy Management and Environmental Sciences Laboratory of U.S. Department of Energy Office of Grand Junction, for their assistance with planning and conducting field sampling activities. We especially thank William Dam, Ray Johnson and Sarah Morris to help to manage the field sampling activities and help to storage and shipping of samples.

We thank the SLAC radiation protection program for their assistance with radioactive sample handling. Eric Nelson, Matthew Latimer, Sam Webb, Courtney Ranch and Ryan Davis, and the technical staff at SSRL are also acknowledged for their technical support during XAS measurements. We also would like to acknowledge Environmental Molecular Sciences Laboratory (EMSL), a DOE-OBER national scientific user facility located at the Pacific Northwest National Laboratory (PNNL), Richland, WA, USA, for assistance with Mössbauer spectroscopy measurements. The authors also thank Cynthia Patty (SLAC) for her great help in the preparation of field sampling and laboratory activities, and Kim Hayes of Department of Civil and Environmental Engineering (University of Michigan) for providing the Fe-sulfide standard samples for Mössbauer spectroscopy.

Appendix A. Supplementary data

Supplementary data to this article can be found online at http://dx.doi.org/10.1016/j.scitotenv.2017.01.109.

References

Benning, L.G., Wilkin, R.T., Barnes, H.L., 2000. Reaction pathways in the Fe–S system below 100 °C. Chem. Geol. 167, 25–51.

Blazejewski, G.A., Stolt, M.H., Gold, A.J., Gurwick, N.P., Groffman, P.M., 2009. Spatial distribution of carbon in the subsurface of riparian zones. Soil Sci. Soc. Am. J. 73 (5), 1733.

Burton, E.D., Bush, R.T., Sullivan, L.A., 2006. Acid-volatile sulfide oxidation in coastal floodplain drains: iron–sulfur cycling and effects on water quality. Environ. Sci. Technol. 40, 1217–1222.

Burton, E.D., Bush, R.T., Sullivan, L.A., Hocking, R.K., Mitchell, D.R.G., Johnston, S.G., Fitzpatrick, R.W., Raven, M.D., McClure, S., Jang, L.Y., 2009. Iron-monosulfide oxidation in natural sediments: resolving microbially mediated S transformations using XANES, electron microscopy, and selective extractions. Environ. Sci. Technol. 43 (9), 3128–3134.

Burton, E.D., Bush, R.T., Johnston, S.G., Sullivan, L.A., Keene, A.F., 2011. Sulfur biogeochemical cycling and novel Fe–S mineralization pathways in a tidally re-flooded wetland. Geochim. Cosmochim. Acta 75 (12), 3434–3451.

Butler, I.B., Rickard, D., 2000. Framboidal pyrite formation via the oxidation of iron (II) monosulfide by hydrogen sulfide. Geochim. Cosmochim. Acta 64, 2665–2672.

Campbell, K.M., Kukkadapu, R.K., Qafoku, N.P., Peacock, A.D., Lesher, E., Williams, K.H., Bargar, J.R., Wilkins, M.J., Figueroa, L., Ranville, J.F., Davis, J.A., Long, P.E., 2012. Geochemical, mineralogical and microbiological characteristics of sediment from a naturally reduced zone in a uranium-contaminated aquifer. Appl. Geochem. 27 (8), 1499–1511.

Cancès, B., Juillot, F., Morin, G., Laperche, V., Alvarez, L., Proux, O., Brown Jr., G.E., Calas, G., 2005. XAS evidence of As(V) association with iron oxyhydroxides in a contaminated soil at a former arsenical pesticide processing plant. Environ. Sci. Technol. 39, 9398–9405.

Canfield, D.E., Raiswell, R., Bottrell, S., 1992. The reactivity of sedimentary iron minerals toward sulfide. Am. J. Sci. 292, 659–683.

Canfield, D.E., Kristensen, E., Thamdrup, B., 2005. Aquatic Geomicrobiology. Elsevier, Amsterdam (640 pp.).

Chaopricha, N.T., Marín-Spiotta, E., 2014. Soil burial contributes to deep soil organic carbon storage. Soil Biol. Biochem. 69, 251–264.

Davis, J.A., Curtis, G.P., Wilkins, M.J., Kohler, M., Fox, P.M., Naftz, D.L., Lloyd, J.R., 2006. Processes affecting transport of uranium in a suboxic aquifer. Phys. Chem. Earth A/B/C 31 (10–14), 548–555.

Druhan, J.L., Steefel, C.I., Conrad, M.E., DePaolo, D.J., 2014. A large column analog experiment of stable isotope variations during reactive transport: I. A comprehensive model of sulfur cycling and $\delta^{34}S$ fractionation. Geochim. Cosmochim. Acta 124, 366–393.

Faye, G.H., 1968. The optical absorption spectra of iron in six-coordinate sites in chlorite, biotite, phlogopite and vivianite. Some aspects of pleochroism in the sheet silicates. Can. Mineral. 9, 403–425.

Findlay, S., 1995. Importance of surface-subsurface exchange in stream ecosystems: the hyporheic zone. Limnol. Oceanogr. 40 (1), 159–164.

Fleet, M.E., 2005. XANES spectroscopy of sulfur in earth materials. Can. Mineral. 43, 1811–1838.

Ford, R.G., Bertsch, P.M., Farley, K.J., 1997. Changes in transition and heavy metal partitioning during hydrous iron oxide aging. Environ. Sci. Technol. 31, 2028–2033.

Hohmann, C., Morin, G., Ona-nguema, G., Guigner, J.-M., Brown Jr., G.E., Kappler, A., 2011. Molecular-level modes of As binding to Fe (III) (oxyhydr)oxides precipitated by the anaerobic nitrate-reducing Fe(II)-oxidizing Acidovorax sp. strain BoFeN1. Geochim. Cosmochim. Acta 75 (17), 4699–4712.

Hua, B., Deng, B., 2008. Reductive immobilization of uranium(VI) by amorphous iron sulfide. Environ. Sci. Technol. 42, 8703–8708.

Hunger, S., Benning, L.G., 2007. Greigite: a true intermediate on the polysulfide pathway to pyrite. Geochem. Trans. 8, 1.

Hyun, S.P., Davis, J.A., Sun, K., Hayes, K.F., 2012. Uranium(VI) reduction by iron(II) monosulfide mackinawite. Environ. Sci. Technol. 46, 3369–3376.

Janot, N., Lezama-PAacheco, J.S., Pham, D.Q., O'Brien, T.M., Hausladen, D., Noël, V., Lallier, F., Maher, K., Fendorf, S., Williams, K.H., Long, P.E., Bargar, J.R., 2016. Physico-chemical heterogeneity of organic-rich sediments in the Rifle aquifer, CO: impact on uranium biogeochemistry. Environ. Sci. Technol. 50 (1), 46–53.

Johnston, J.H., Cardile, C.M., 1987. Iron substitution in montmorillonite, illite and glausonite by ^{57}Fe Mössbauer spectroscopy. Clay Clay Miner. 35 (3), 170–176.

Juillot, F., Marechal, C., Morin, G., Jouvin, D., Cacaly, S., Telouk, P., Benedetti, M.F., Ildefonse, P., Sutton, S., Guyot, F., Brown Jr., G.E., 2011. Contrasting isotopic signatures between anthropogenic and geogenic Zn and evidence for post-depositional fractionation processes in smelter-impacted soils from Northern France. Geochim. Cosmochim. Acta 75, 2295–2308.

Karickhoff, S.W., Bailey, G.W., 1973. Optical absorption spectra of clay minerals. Clay Clay Miner. 21, 59–70.

Kornicker, W.A., Morse, J.W., 1991. The interactions of divalent cations with the surface of pyrite. Geochim. Cosmochim. Acta 55, 2159–2172.

Kukkadapu, R.K., Zachara, J.M., Fredrickson, J.K., McKinley, J.P., Kennedy, D.W., Smith, S.C., Dong, H., 2006. Reductive biotransformation of Fe in shale-limestone saprolite containing Fe(III)-oxides and Fe(II)/Fe(III) phyllosilicates. Geochim. Cosmochim. Acta 70 (14), 3662–3676.

Lair, G.J., Zehetner, F., Fiebig, M., Gerzabek, M.H., Van Gestel, C.A.M., Hein, T., Hohensinner, S., Hsu, P., Jones, K.C., Jordan, G., Koelmans, A.A., Poot, A., Slijkerman, D.M.E., Totsche, K.U., Bondar-Kunze, E., Barth, J.A.C., 2009. How do long-term development and periodical changes of river-floodplain systems affect the fate of contaminants? Results from European rivers. Environ. Pollut. 157, 3336–3346.

Luther III, G.W., 1991. Pyrite synthesis via polysulfide compounds. Geochim. Cosmochim. Acta 55, 2839–2849.

Lynch, S.F.L., Batty, L.C., Byrne, P., 2014. Environmental risk of metal mining contaminated river bank sediment at redox-transitional zones. Fortschr. Mineral. 4, 52–73.

Miller, M.P., Boyer, E.W., McKnight, D.M., Brown, M.G., Gabor, R.S., Hunsaker, C.T., Iavorivska, L., Inamdar, S., Johnson, D.W., Kaplan, L.A., Lin, H., McDowell, W.H., Perdrial, J.N., 2016. Variation of organic matter quantity and quality in streams at Critical Zone Observatory watersheds. Water Resour. Res. 52, 3547–3562.

Morse, J.W., Arakaki, T., 1993. Adsorption and coprecipitation of divalent metals with mackinawite. Geochim. Cosmochim. Acta 57, 3635–3640.

Naiman, R.J., Décamps, H., 1997. The ecology of interfaces: riparian zones. Annu. Rev. Ecol. Syst. 28, 621–658.

Nielsen, T., Andersen, F.O., 2003. Phosphorus dynamics during decomposition of mangrove (*Rhizophora apiculata*) leaves in sediments. J. Exp. Mar. Biol. Ecol. 293, 73–88.

Noël, V., Marchand, C., Juillot, F., Ona-Nguema, G., Viollier, E., Marakovic, G., Olivi, L., Delbe, L., Gelebart, F., Morin, G., 2014. EXAFS analysis of iron cycling in mangrove sediments downstream a lateritized ultramafic watershed (Vavouto Bay, New Caledonia). Geochim. Cosmochim. Acta 136, 211–228.

Otero, X.L., Vidal-Torrado, P., Calvo de Anta, R., Macías, F., 2005. Trace elements in biodeposits and sediments from mussel culture in the ría de Arousa (Galicia. NW Spain). Environ. Pollut. 136, 119–134.

Please cite this article as: Noël, V., et al., Understanding controls on redox processes in floodplain sediments of the Upper Colorado River Basin, Sci Total Environ (2017), http://dx.doi.org/10.1016/j.scitotenv.2017.01.109

Pantke, C., Obst, M., Benzerara, K., Morin, G., Ona-Nguema, G., Dippon, U., Kappler, A., 2012. Green rust formation during Fe(II) oxidation by the nitrate-reducing *Acidovorax* sp. strain BoFeN1. Environ. Sci. Technol. 46, 1439–1446.

Parkman, R.H., Charnock, J.M., Bryan, N.D., Livens, F.R., Vaughan, D.J., 1999. Reactions of copper and cadmium ions in aqueous solution with goethite, lepidocrocite, mackinawite, and pyrite. Am. Mineral. 84, 407–419.

Peretyazhko, T.S., Zachara, J.M., Kukkadapu, R.K., Heald, S.M., Kutnyakov, I.V., Resch, C.T., Arey, B.W., Wang, C.M., Kovarik, L., Philips, J.L., Moore, D.A., 2013. Pertechnetate (TcO_4^-) reduction by reactive ferrous iron forms in naturally anoxic, redox transition zone sediments from the Hanford site. Geochim. Cosmochim. Acta 92, 48–66.

Pinay, G., Décamps, H., Chauvet, E., Fustec, E., 1991. Functions of ecotones in fluvial systems. In: Naiman, R.J., Décamps, H. (Eds.), Ecology and Management of Aquatic-Terrestrial Ecotones. UNESCO/Paris and Parthenon Publishing Group, Paris, pp. 141–170.

Prietzel, J., Botzaki, A., Tyufekchieva, N., Brettholle, M., Thieme, J., Klysubun, W., 2011. Sulfur speciation in soil by S K-edge XANES spectroscopy: comparison of spectral deconvolution and linear combination fitting. Environ. Sci. Technol. 45 (7), 2878–2886.

Pyzik, A.J., Sommer, S.E., 1981. Sedimentary iron monosulfide: kinetics and mechanism of formation. Geochim. Cosmochim. Acta 45, 687–698.

Qafoku, N.P., Kukkadapu, R.K., McKinley, J.P., Arey, B.W., Kelly, S.D., Wang, C., Resch, C.T., Long, P.E., 2009. Uranium in framboidal pyrite from a naturally bioreduced alluvial sediment. Environ. Sci. Technol. 43 (22), 8528–8534.

Qafoku, N.P., Gartman, B.N., Kukkadapu, R.K., Arey, B.W., Williams, K.H., Mouser, P.J., Heald, S.M., Bargar, J.R., Janot, N., Yabusaki, S., Long, P.E., 2014. Geochemical and mineralogical investigation of uranium in multi-element contaminated, organic-rich subsurface sediment. Appl. Geochem. 42, 77–85.

Rancourt, D.G., Ping, J.Y., 1991. Voigt-based methods for arbitrary-shape static hyperfine parameter distributions in Mössbauer spectroscopy. Nucl. Instrum. Methods Phys. Res., Sect. B 58, 85–97.

Ravel, B., Newville, M., 2005. ATHENA, ARTEMIS, HEPHAESTUS: data analysis for X-ray absorption spectroscopy using IFEFFIT. J. Synchrotron Radiat. 12, 537–541.

Rickard, D., 1975. Kinetics and mechanism of pyrite formation at low temperatures. Am. J. Sci. 275, 636–652.

Rickard, D., 1997. Kinetics of pyrite formation by the H_2S oxidation of iron(II) monosulfide in aqueous solution between 25 and 125 °C: the rate equation. Geochim. Cosmochim. Acta 61, 115–134.

Rickard, D., Luther III, G.W., 1997. Kinetics of pyrite formation by the H_2S oxidation of iron(II) monosulfide in aqueous solution between 25 and 125 °C: the mechanism. Geochim. Cosmochim. Acta 61, 135–147.

Rickard, D., Luther, G.W., 2007. Chemistry of iron sulfides. Chem. Rev. 107 (2), 514–562.

Schippers, A., Sand, W., 1999. Bacterial leaching of metal sulfides proceeds by two indirect mechanisms via thiosulfate or via polysulfides and sulfur. Appl. Environ. Microbiol. 65, 319–321.

Schoonen, M.A.A., Barnes, H.L., 1991. Reactions forming pyrite and marcasite from solutions: II. FeS precursors below 100 °C. Geochim. Cosmochim. Acta 55, 1505–1514.

Schulz-Zunkel, C., Jörg Rinklebe, J., Bork, H.-R., 2015. Trace element release patterns from three floodplain soils under simulated oxidized–reduced cycles. Ecol. Eng. 83, 485–495.

Shuman, L.M., 1997. Adsorption of Zn by Fe and Al hydrous oxides as influenced by aging and pH. Soil Sci. Soc. Am. J. 41, 703–706.

Tabacchi, E., Correll, D.L., Hauer, R., Pinay, G., Planty-Tabacchi, A.M., Wissmar, R.C., 1998. Development, maintenance and role of riparian vegetation in the river landscape. Freshw. Biol. 40, 497–516.

Tockner, K., Stanford, J.A., 2002. Riverine flood plains: present state and future trends. Environ. Conserv. 29, 308–330.

Tockner, K., Lorang, M.S., Stanford, J.A., 2010. River flood plains are model ecosystems to test general hydrogeomorphic and ecological concepts. River Res. Appl. 26 (1), 76–86.

Veeramani, H., Scheinost, A.C., Monsegue, N., Qafoku, N.P., Kukkadapu, R., Newville, M., Lanzirotti, A., Pruden, A., Murayama, M., Hochella, M.F., 2013. Abiotic reductive immobilization of U(VI) by biogenic mackinawite. Abiotic reductive immobilization of U(VI) by biogenic mackinawite. Environ. Sci. Technol. 47, 2361–2369.

Weber, F.-A., Voegelin, A., Kaegi, R., Kretzschmar, R., 2009. Contaminant mobilization by metallic copper and metal sulphide colloids in flooded soil. Nat. Geosci. Lett. 2, 267–271.

Wei, D., Osseo-Asare, K., 1997. Aqueous synthesis of finely divided pyrite particles. Colloids Surf. A Physicochem. Eng. Asp. 121 (1), 27–36.

Wilkin, R.T., Barnes, H.L., 1996. Pyrite formation by reactions of iron monosulfides with dissolved inorganic and organic sulfur species. Geochim. Cosmochim. Acta 60, 4167–4179.

Williams, K.H., Long, P.E., Davis, J.A., Wilkins, M.J., N'Guessan, A.L., Steefel, C.I., Yang, L., Newcomer, D.R., Spane, F.A., Kerkhof, L.J., Mcguinness, L., Dayvault, R., Lovley, D.R., 2011. Acetate availability and its influence on sustainable bioremediation of uranium-contaminated groundwater. Geomicrobiol J. 28 (5–6), 519–539.

Please cite this article as: Noël, V., et al., Understanding controls on redox processes in floodplain sediments of the Upper Colorado River Basin, Sci Total Environ (2017), http://dx.doi.org/10.1016/j.scitotenv.2017.01.109